Thermoelastic and electronic properties of quasi-one-dimensional defects in tellurium

1991 J. Phys.: Condens. Matter 3 307

(http://iopscience.iop.org/0953-8984/3/3/006)

J. Phys.: Condens. Matter 3 (1991) 307–328. Printed in the UK

Thermoelastic and electronic properties of quasi-one-dimensional defects in tellurium

W Baier and H Köhler
Physikalisches Institut, Universität Würzburg, 8700 Würzburg, Federal Republic of Germany

Received 15 September 1989

Abstract. The thermoelastic effect decreases with increasing concentration of linear defects ('α edge dislocations') generated by plastic deformation. Hence, an improvement of binding may be assumed. We interpret the linear defects as resulting from interstitial atoms, six per lattice constant c. Binding is increased by additional σ and π bonds, with components perpendicular and parallel to the trigonal chains. It is shown experimentally that the linear interstitial defects (LID) are active as acceptors, causing quasi-metallic p-type conduction. This may be realized from the assumption that, in the cylindrical LID potential, a two-dimensional interaction yields equivalent eigenstates and a quasi-free motion parallel to the linear defects. The model, in addition, allows the interpretation of defect-induced cyclotron resonance inactive-mode absorption in an unconstrained manner, as a result of the acceptor effect of the quasi-one-dimensional defects. Furthermore, the angular dependence and fine structure of resonant scattering in the magneto-impurity effects under hot carrier conditions of built-in group V atoms can be explained quantitatively.

1. Introduction

Tellurium is a widely investigated elemental semiconductor. It possesses many interesting properties, though a series of problems appear to be unsolved to date. The Conference on the Physics of Selenium and Tellurium, held in Königstein in 1979 (Grosse and Gerlach 1979), marked a reduction in research in this field, as can be seen from the reduced amount of research activity world-wide since then. Nevertheless, the p-type doping mechanism, chemical bonding, cyclotron resonance inactive-mode absorption, etc., are examples worthy of further investigation, though an enormous variety of results are available. However, not infrequently has the quality of the samples (growth and preparation of the crystals) played a crucial role in the investigations and their interpretation.

Therefore, we present here an alternative view of the influence of crystal defects on the properties of real tellurium. Crystals of the highest quality have been prepared—undoped and doped—and the density of linear defects ('dislocations') subsequently increased by controlled plastic deformation. At any stage the free-carrier (hole) concentration is determined from the Hall effect at low temperatures, and the variation of the average binding potential is deduced from the thermoelastic properties of the samples.

0953-8984/91/030307 + 22 $03.50

The thermoelastic effect (TEE) (Swalin 1972, Köhler 1978) has been shown to be a powerful tool for the investigation of the non-stoichiometry in Bi_2Te_3, causing point defects of tellurium, and chemical bonding (Dato and Köhler 1984). The investigation of non-stoichiometry in SnTe and of the effect of composition of $Bi_{1-x}Sb_x$ crystals on the thermoelastic properties has revealed interesting dependences on the respective parameters. The TEE allows one to determine the thermal expansion coefficient, even on small samples, by measurement of a reversible stress-induced temperature variation, and the application of hydrostatic pressure yields a favourable experimental procedure in the case of easily deformable tellurium. Since any phase of matter, forming a surface (i.e. solid or liquid), exhibits a thermoelastic effect, as the stress-transferring medium we choose water at 4 °C, where its thermal expansion coefficient and its thermoelastic effect both vanish completely, and a clear separation of the crystal's influence may be achieved (order of magnitude 1 mK bar^{-1}). It is shown that, particularly, the concentration of quasi-one-dimensional defects (here '*a* edge dislocations') influences the magnitude of the TEE.

2. Theoretical background

2.1. Thermoelastic effect

The thermoelastic effect is described by Swalin (1972). However, an even more direct deduction may be obtained by use of the enthalpy H with independent variables S (entropy) and p (pressure):

$$\begin{aligned} H &= U + pV \\ \mathrm{d}H &= \mathrm{d}U + p\,\mathrm{d}V + V\,\mathrm{d}p \end{aligned} \tag{1}$$

with V = volume, U = internal energy and T = temperature. The first law of thermodynamics yields

$$\mathrm{d}H = T\,\mathrm{d}S + V\,\mathrm{d}p \tag{2}$$

and, therefore, $T = (\partial H/\partial S)_p$ and $V = (\partial H/\partial p)_S$ hold. Integrability of H demands that

$$\partial^2 H/\partial p \partial S = \partial^2 H/\partial S \partial p$$

or

$$(\partial T/\partial p)_S = (\partial V/\partial S)_p = (\partial V/\partial T)_p/(\partial S/\partial T)_p. \tag{3}$$

The numerator in the last expression of equation (3)

$$(\partial V/\partial T)_p = V\alpha \tag{4}$$

is defined by the isobaric thermal expansion coefficient α and the denominator

$$(\partial S/\partial T)_p = c_p/T \tag{5}$$

by the isobaric specific heat c_p. Hence, equation (3) becomes

$$(\partial T/\partial p)_S = \alpha T/(c_p/V) = \gamma\beta T/\kappa \tag{6}$$

where γ is the Grüneisen parameter, β the isothermal compressibility and $\kappa = c_p/c_V \simeq 1$ for a solid. For a particular average temperature T and a known value of c_p/V, the

isobaric thermal expansion coefficient α may be determined when, in a reversible process ($dS = 0$), the temperature variation ΔT is measured on application (or release) of a stress Δp. Since thermal transport occurs, ΔT has to be extrapolated towards the switching time $t = 0$ of the stress,

$$\lim_{t \to 0} (\Delta T/\Delta p)|_S = \Delta T(0)/\Delta p \tag{7}$$

where complete reversibility is ascertained by comparison of the results for $\Delta p \gtrless 0$ and $|\Delta p| =$ constant. For strongly anisotropic chemical bonds—as realized in tellurium—α represents an average over all bonds, but the weakest bonds certainly contribute the maximum effect, which is easily verified in the following linear approximation.

2.2. Anharmonicity of binding potential

Thermodynamic equilibrium is reached at the minimum of the free energy F. Without external stress the binding potential φ around the equilibrium distance r_0 for $T = 0$ may be developed as

$$\varphi = \varphi(r_0) + \tfrac{1}{2} f_h u_n^2 + \tfrac{1}{6} f_{anh} u_n^3 + O(u_n^4) \tag{8}$$

with $f_h = (\partial^2 \varphi/\partial r^2)|_{r_0}$, $f_{anh} = (\partial^3 \varphi/\partial r^3)|_{r_0}$ and $u_n =$ the displacement of the lattice element n from r_0. The repulsive part in the total potential φ should be rather isotropic; the contribution leading to binding in Te is certainly anisotropic. Therefore, for the weakest bonds, f_{anh} in equation (8) should be higher than f_h. For $T > 0$ in a linear model the equilibrium distance is $r^* = (1 + \varepsilon) r_0$, and the expansion around $r = r^*$ becomes

$$\begin{aligned} \varphi &= \varphi(r^*) + \left.\frac{\partial \varphi}{\partial r}\right|_{r^*} u_n + \frac{1}{2} \left.\frac{\partial^2 \varphi}{\partial r^2}\right|_{r^*} u_n^2 + \frac{1}{6} \left.\frac{\partial^3 \varphi}{\partial r^3}\right|_{r^*} u_n^3 + \ldots \\ &= \varphi(r^*) + (f_h \varepsilon r_0 + \tfrac{1}{2} f_{anh} r_0^2 \varepsilon^2) u_n \\ &\quad + \tfrac{1}{2}(f_h + f_{anh} r_0 \varepsilon) u_n^2 + \tfrac{1}{6} f_{anh} u_n^3 + \ldots . \end{aligned} \tag{9}$$

Since $F = -k_B T \ln Z$, where Z is the partition function, $(\partial F/\partial \varepsilon)_T = 0$ yields

$$\varepsilon = -(f_{anh}/2 f_h^2 r_0) k_B T \tag{10}$$

and $\alpha = (\partial \varepsilon/\partial T)_p$ becomes

$$\alpha = -(k_B/2 r_0 f_h) f_{anh}/f_h \tag{11}$$

in a lowest-order approximation (contributions up to u_n^3 in equation (8)). Therefore, the TEE contribution should be highest for the weakest bonds, since the variations of r_0 and f_h in the denominator of the prefactor in equation (11) with the strength of binding are opposite and $|f_{anh}/f_h|$ increases for a weakening of the binding ($f_{anh} < 0$). Any defect-induced, average alteration of the weakest bonds, therefore, should show up in a distinct variation of the TEE. It is the purpose of this paper to try to realize a variation of $\Delta T(0)/\Delta p$ with a preparational parameter of the tellurium crystals.

3. Experimental methods

The tellurium single crystals were grown by the Czochralski method, with and without chemical doping. Preparation of the samples was performed by acid string sawing and

etching (Honeywell etch: 100 g CrO_3, 266 g H_2O, 132 g HCl (32%)). The geometry for the TEE measurements was chosen as about 1 cm^2 basis plane and roughly 10 mm height parallel to the ***c*** axis. This volume was adequate in order to achieve sufficiently high relaxation times for the temperature deviation $\Delta T(t)$. The Hall effect was investigated on smaller pieces (about $8 \times 3 \times 1.5$ mm^3; gold wires soldered by indium) from the same crystal volume after deformation of the samples, i.e. the rest volume is reduced after every deformation step and TEE measurement.

The Ni–NiCr thermocouple (50 μm diameter) for the determination of ΔT was spot-welded to the crystals; the thermopower was amplified by an Amplispot Nanovolt Galvanometer of Burster/Sefram and plotted as a function of time by a Hewlett Packard 7047A X–Y–t recorder. A pressure chamber of about 65 cm^3 volume was used, allowing experiments up to about 300 bar. This hydrostatic pressure is sufficiently small in order to avoid the metallic phase transition at 38 kbar (Jamieson and McWham 1965, Parthasarathy and Holzapfel 1988). The experimental set-up was checked by investigation of the TEE of the water medium between about 3 and 21 °C. The thermal expansion coefficient of water is reproduced. A schematic drawing of the pressure cell is shown in figure 1.

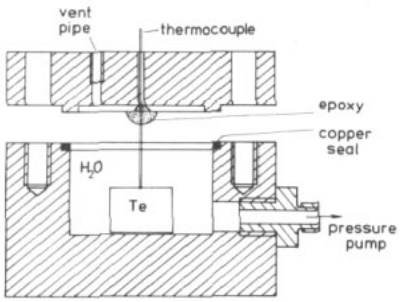

Figure 1. Schematic drawing of pressure cell with Te sample and thermocouple.

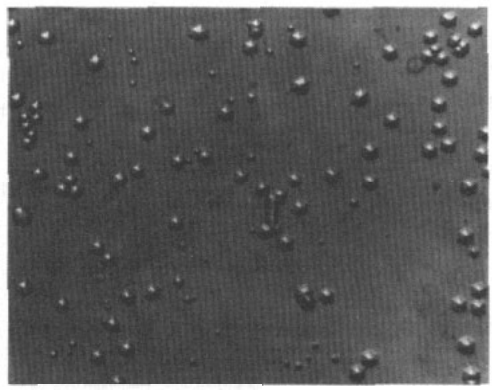

Figure 2. Etch pits on trigonal basis plane of the non-deformed crystal HwTe 99. The figure corresponds to a section of area 174×129 μm^2.

Plastic deformation was achieved at room temperature with a constant deformation velocity of about 3 $\mu m\ s^{-1}$, where the force was applied normal to the $(01\bar{1}0)$ and $(0\bar{1}10)$ planes. The amount of deformation was controlled by a microscope in steps of about 2%. The duplex ***a*** glide yields ***a*** edge dislocations and other defects (Faivre 1974, von Alpen 1973), the latter of which heal up after room-temperature 'annealing' for some days. A delayed start of the experiments by some days ensures that the plastic deformation has increased the density of ***a*** edge dislocations exclusively. The density of dislocations was determined by etching of the basis planes (Doukhan and Farvaque 1971) at 150 °C and optical counting of the etch pits, where a 1 : 1 correlation of etch pits and dislocations may be assumed (Doukhan and Farvaque 1971, Broniatowski and Faivre 1974, Naukkarinen 1972, Kalinski and Lehmann 1976). A typical Te surface

(trigonal plane) with etch pits is shown in figure 2. The dislocation densities were evaluated between about 10^4–10^5 cm^{-2} (without deformation) and 10^7 cm^{-2} (after 4% deformation).

The Hall constant was determined at 4.2 K up to $B = 10.3$ T ($\boldsymbol{B} \| \boldsymbol{c}$) on smaller samples cut from the same crystal piece as investigated in the TEE measurements. For high magnetic fields ($R_{H\infty}$ = saturation value of the Hall constant), the hole concentration p^* may be deduced fairly well from

$$p^* = (eR_{H\infty})^{-1}. \tag{12}$$

The influence of chemical doping and of the density of dislocations on R_H was investigated. For undoped and sufficiently pure samples, the density of a edge dislocations yields a clear connection with the hole concentration at 4.2 K. This is discussed below.

4. Results

In figure 3 the pressure-induced temperature deviation ΔT is shown as a function of time, where the average temperature ϑ of the sample and the water medium is a parameter for switching of an non-variable pressure $\Delta p = 72.5 \pm 2.5$ bar at $t = 0$. In

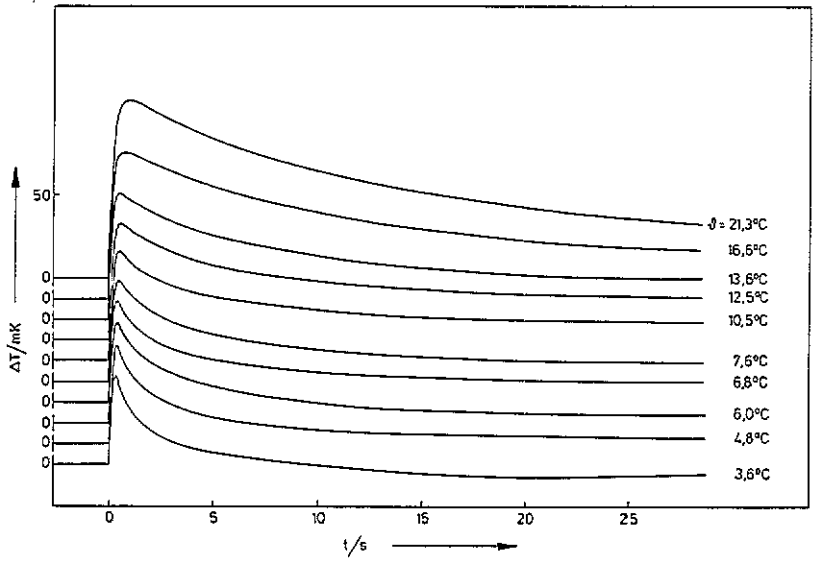

Figure 3. Temporal variation of temperature deviation $\Delta T(t)$ of a Te sample in water between 3.6 and 21.3 °C. The pressure $\Delta p = 72.5 \pm 2.5$ bar is applied at each $t = 0$.

general, effects from both the Te sample and H_2O are superimposed with different magnitudes and time constants (the influence of the pressure chamber itself is negligible at a sufficient distance from the walls). As the total effect changes sign at $t \simeq 10$ s for $\vartheta =$

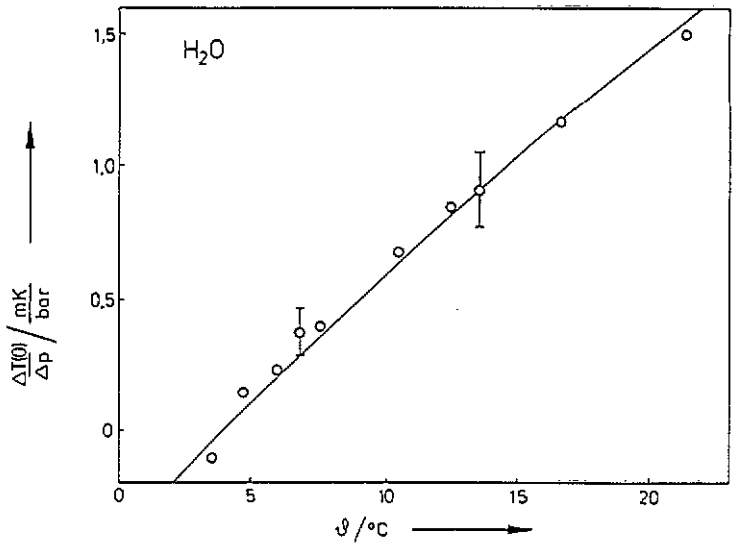

Figure 4. The TEE of water after extrapolation towards $t = 0$ as a function of the average temperatue ϑ. The experimental results (○) are deduced from figure 3 (for discussion, see text). The full curve is calculated from the well known data for α and c_p for H_2O.

3.6 °C, an essentially higher time constant is realized for the water medium (about 3.5 mol) than for the sample (about 0.05 mol). The effect of Te is essentially unchanged in figure 3 as a function of ϑ, and $\Delta T(0)$ for $t = 0$ may be extrapolated from the almost exponential $\Delta T(t)$ decay, at least for the first few seconds, as a result of thermal conduction after the turn-on process.

Though it is obvious that a measurement at or near 4 °C is recommended for the evaluation, the influence of H_2O may be deduced from the results of figure 3 on the assumption that the effect of the sample has roughly decayed at $t = 15$ s, while that of water is still finite without remarkable relaxation. This evaluation is shown in figure 4 (open circles), where the full curve represents the theoretical expectation from the well known data of α and c_p for H_2O. In particular, a zero TEE and a reversal of sign for water are obtained at $\vartheta \simeq 4$ °C.

In figure 5, $\Delta T(t)$ and $\Delta p(t)$ are drawn for a Te sample (HwTe 98) at about 4 °C. The switching of the pressure is assumed to occur immediately in comparison with the thermal and electronic relaxation times of the system. The TEE is shown to be reversible as expected for sufficiently low applied hydrostatic pressure. For the decay of $\Delta T(t)$ an exponential law is obtained, approximately

$$\Delta T(t) = \Delta T(0)\, e^{-\lambda t} \tag{13}$$

within the first few seconds, which is shown in figure 6 for the same sample as in figure 5. From the inhomogeneous thermal conduction, a deviation from equation (13) has to be expected. Nevertheless, a rather reliable extrapolation towards $t = 0$ is possible, where the systematic deviation should be rather small and yield the same relative error for any Δp. In a comparison with results obtained on different samples, this relative uncertainty should cancel out almost completely. The slopes of the straight lines in figure

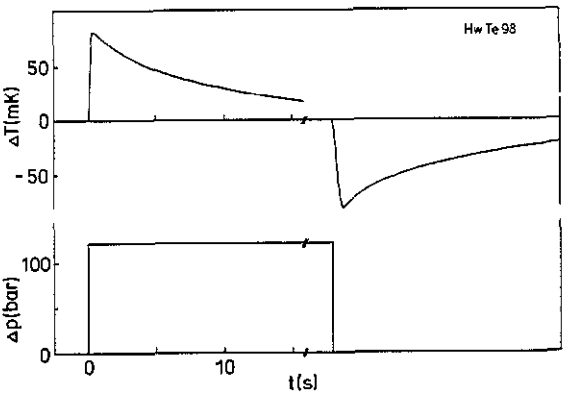

Figure 5. Temperature deviation $\Delta T(t)$ and pressure profile $\Delta p(t)$ for $\vartheta \approx 4$ °C for the Te sample HwTe 98. The rise of $|\Delta T(t)|$ is influenced by the characteristic time constant of the system.

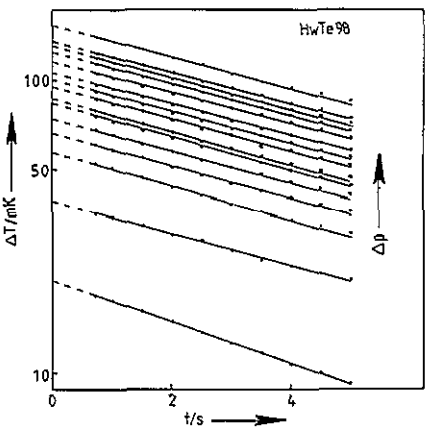

Figure 6. Plot of ΔT in a logarithmic scale as a function of time for sample HwTe 98 and different pressures $\Delta p = 25$–200 bar.

6 are approximately the same, except for some small increase at low Δp, unimportant for the whole $\Delta T(0)$ data as a function of Δp in figure 7.

The sum of all results for various samples and deformation steps as a function of the primary hole concentration p^* (without intentional plastic deformation) and for the dislocation density N_{dis} before (left) and after plastic deformation is plotted in figure 8. The curves between the circles for $p^* =$ constant indicate the preparational steps. A possible variation of p^* by plastic deformation is not considered. Primarily, neglecting the highest and lowest chemical doping ranges (highest and lowest p^* in figure 8), the overall tendency is a reduction of the TEE with increasing dislocation density induced by plastic deformation. The increase at the highest doping levels (p^*) should not be considered as representative, as a result of the possibility of segregation of chemical doping material within the samples, leading to an uncontrollable defect situation. For the purest (undoped) sample investigated, the additional effect of doping by the linear defects induced by plastic deformation (to be discussed below) might play a relatively larger role than for the doped samples with higher initial p^*. The average decrease of

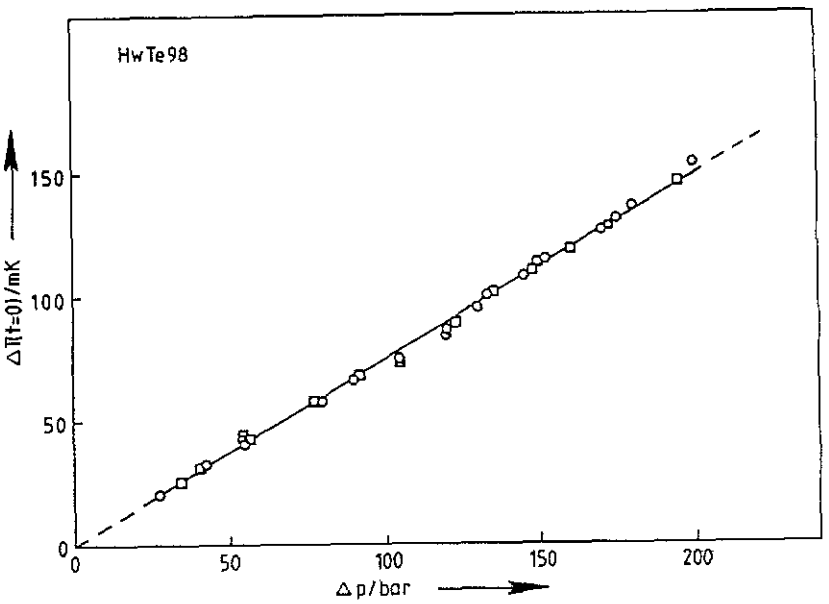

Figure 7. Extrapolated values $\Delta T(t = 0)$ as a function of Δp for sample HwTe 98. Reversibility is demonstrated by coincidence of the results (within the error margins) for application (○) and release (□) of pressure.

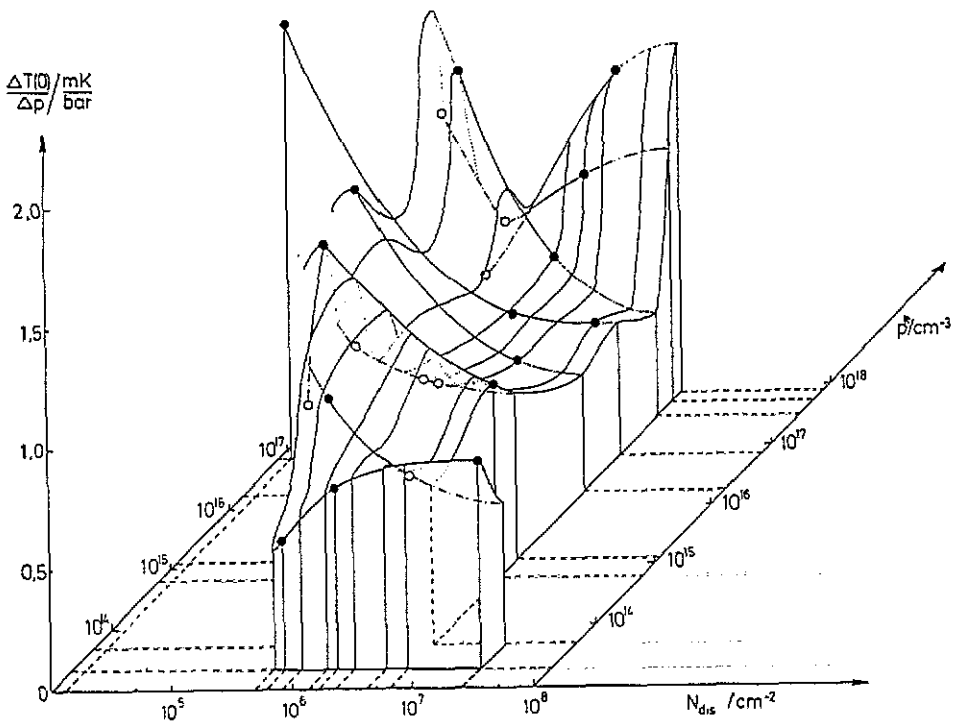

Figure 8. Summary results of $\Delta T(0)/\Delta p$ in a perspective three-dimensional plot for different samples with different hole concentrations p^* before intentional plastic deformation. For each sample N_{dis} is increased in several steps of preparation by plastic deformation. For discussion, see text.

the TEE, proportional to the anharmonic part of the average binding (primarily of the weakest bonds), with N_{dis} indicates solidification of the samples by plastic deformation, particularly by production of *a* edge dislocations.

Finally, the variation of p^* (determined at 4.2 K) as a function of the dislocation density was investigated. The results for some doped samples are shown in figure 9. Pure and doped samples were used. The preparational steps (two each) are connected by different lines. It may be deduced that the purest samples show a maximum dependence $p^* = p^*(N_{dis})$, and there is a negligible effect at highest doping levels, at least in the range investigated. As can be seen, a limiting straight line with slope 1 appears to exist where the hole concentration $p^*_{dis}(N_{dis})$, induced by dislocations, approaches $p^*_{dis} \sim N_{dis}$.

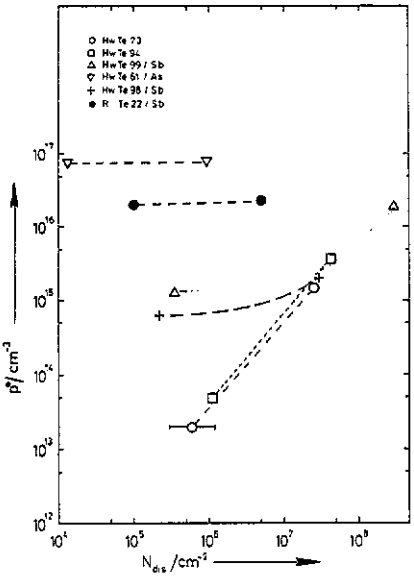

Figure 9. Variation of hole concentration p^* as a function of plastic deformation (N_{dis}) for pure and doped samples: before (left) and after (right) intentional deformation.

In order to find the respective relations for pure and weakly doped samples, only the results for $p^* \simeq p^*_{dis}$ ($p^*_{imp} \ll p^*_{dis}$) were plotted as a function of N_{dis} in figure 10.. Since the Hall constant and the counting of dislocations, i.e. of etch pits, possess some uncertainty, a description of the experimental results by the straight line in figure 10,

$$p^* = p^*_{dis} = 3N_{dis}/c = 5.04 \times 10^7 \, N_{dis} \ \mathrm{cm}^{-1} \tag{14}$$

appears to be reasonable. Here c is the lattice constant in the direction of the trigonal axis. It is obvious that the *a* edge dislocations yield a contribution to the hole concentration, i.e. they are electronically active. For our samples, clustering of the dislocations could be avoided up to the highest degrees of deformation investigated (N_{dis} about $10^7 \ \mathrm{cm}^{-2}$). N_{dis} saturates as a function of plastic deformation (figure 11).

5. Structure of linear defects parallel to the *c* axis

The minimum concentration of linear defects along the *c* axis in tellurium single crystals ever realized is about $10^4 \ \mathrm{cm}^{-2}$. Their density may be increased by plastic deformation.

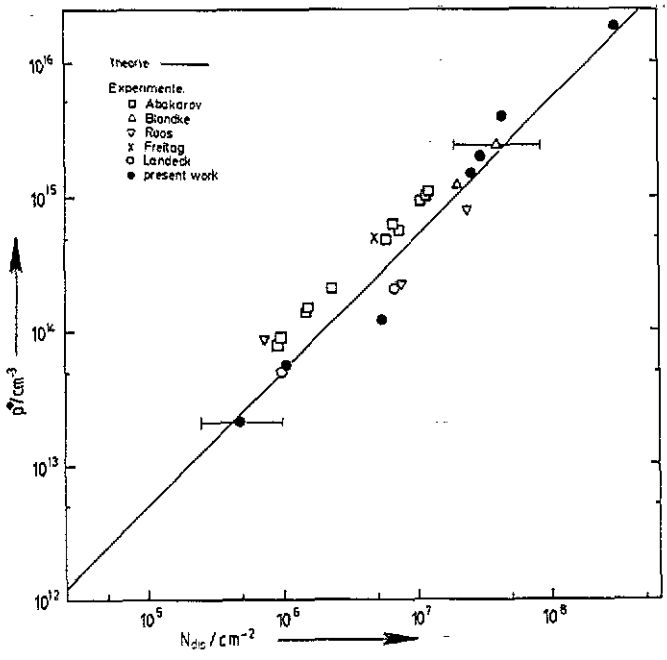

Figure 10. Dependence of hole concentration on N_{dis} for pure and weakly doped samples. Some of the results were taken from other work: (□) Abokarov *et al* (1973); (△) Blondke (1975); (▽) Roos (1975); (×) Freitag (1977); (○) Landeck (1977); (●) present work. The straight line represents equation (14).

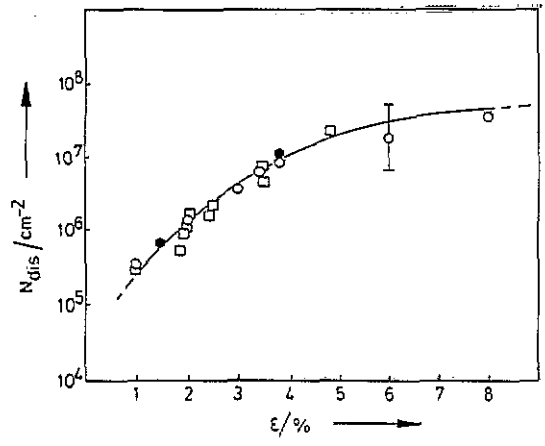

Figure 11. Concentration of dislocations N_{dis} as a function of the degree of plastic deformation ε: (□) present work; (●) Landeck (1977); (○) Freitag (1977).

The model of Doukhan (1971) starts from the assumption that *a* edge dislocations are formed, though the respective Burger's vector could never be proven to exist (actually this was realized for *a* screw dislocations, e.g. by Doukhan *et al* (1969)). Nevertheless, such edge dislocations were assumed to develop, the model of which is shown in figure 12 (Doukhan 1971). Obviously, in the core of the dislocation the crystal is widened, though it usually originates from a plastic crystal compression. In this picture the compressibility of the samples should increase with the linear defect concentration, which does not fit the results obtained here for the TEE. An increase of crystal binding by defect generation cannot be understood on this basis, since even for 10^8 defects/cm^2

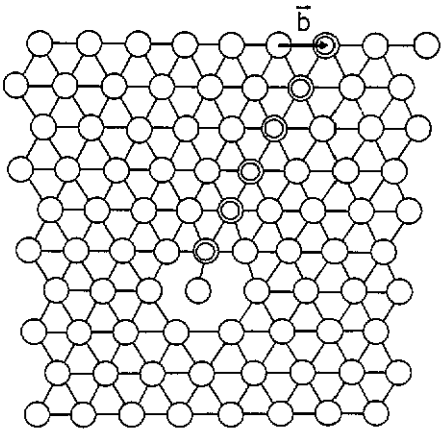

Figure 12. The *a* edge dislocation model of Doukhan (1971). For discussion, see text.

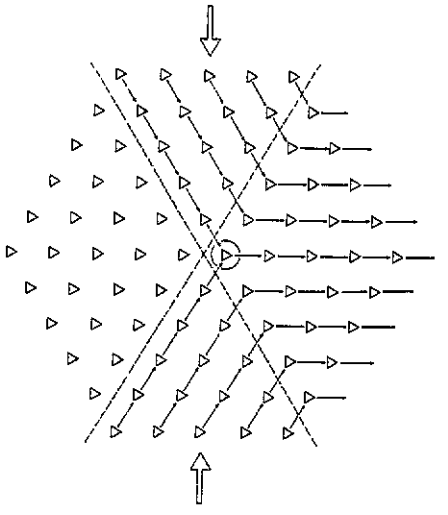

Figure 13. New model for plastic deformation perpendicular to trigonal axis. Large open arrows indicate external forces; small arrows symbolize displacement of tellurium chains (open triangles). Around the encircled area, odd Te atoms enter into interstitial sites by displacement. The broken straight lines indicate binary directions.

their average distance is still more than 10^3 lattice spacings and the binding within the trigonal chains is unaffected.

Therefore, we propose that the linear defects parallel to the *c* axis (usually designated as *a* edge dislocations) are composed of three *a* edge dislocations in such a way that the sum of the Burger's vectors adds up to zero. We assume that—instead of a widening of the crystal around the core—a compression causes interstitial atoms in the lattice. This is shown schematically in figure 13. The trigonal chains (open triangles) are shifted by an external force (large open arrow) along the two binary directions (– – –; duplex *a* glide), indicated by small arrows, by two lattice spacings, yielding an accumulation of two additional trigonal tellurium chains within the vicinity of the area encircled in figure 13. The result is a displacement of six tellurium atoms per lattice spacing *c* into six equivalent interstitial sites. This effect—induced by a compression—is highly probable since the tellurium lattice is a slightly distorted primitive cubic lattice and approximate BCC interstitials seem to make sense and allow a modification of the binding.

Before this influence may be discussed, a repetition of the binding proposed for undisturbed Te is necessary. Grosse (1969) cites the diploma thesis of Drope (1968), where a combination of sp^2, sp and p states is discussed for the intra- and inter-chain binding of tellurium. We follow this designation in figure 14, where nearest-neighbour inter-chain binding in the *xy* plane is managed by two sp_xp_y hybrids (sp_xp_y, $sp_x\bar{p}_y$; σ bonds). The respective $s\bar{p}_xp_z$ and $s\bar{p}_x\bar{p}_z$ orbitals (inclined to the *xy* plane) aim approximately at more distant neighbours in second-order neighbouring chains. The distance of 6.28 Å does not allow effective σ binding to form. In contrast to Grosse (1969), instead of additional sp_x states, we propose the occupation of sp_z and $s\bar{p}_z$ hybrids (or p_z) and p_y states in addition, both forming π bonds with more range than nearest neighbours. It

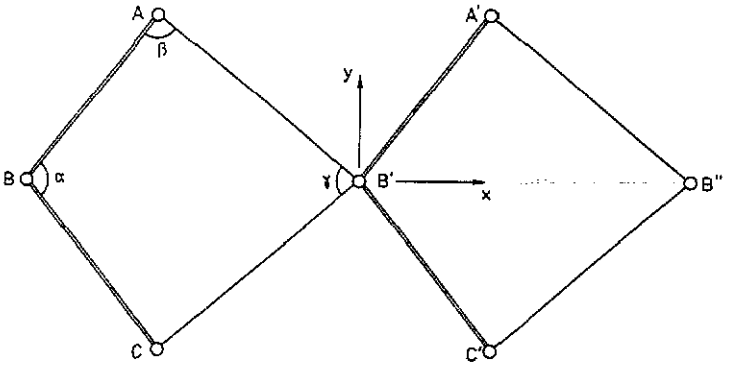

Figure 14. Tellurium atoms (○) in xy plane (Grosse 1969) belonging to the same (A, B, C) and different trigonal chains (e.g. B, B', B", ...). The σ bonds between A'B' and B'C' ($sp_x p_x$ and $sp_x \bar{p}_x$ with respect to B') are indicated by double straight lines. The atomic distances are: $d_{AB} = d_1 = 2.86$ Å, $d_{AB'} = d_2 = 3.48$ Å, $d_{BB'} = d_3 = 4.45$ Å and $d_{AC} = d_4 = 4.46$ Å. The actual binding angles deviate from 90°: $\alpha = 102.6°$, $\beta = 88.9°$ and $\gamma = 79.6°$. The x direction corresponds to a binary axis; e_z is not parallel to c.

may be assumed that the six outer tellurium electrons in the perfect crystal occupy the orbitals mentioned except $s\bar{p}_x p_z$ and $s\bar{p}_x \bar{p}_z$ (as a result of negligible overlap with neighbouring wavefunctions).

Formation of a linear interstitial defect (LID) parallel to the c axis automatically yields an increase of binding due to the intermediate position of the interstitial atom between the more distant neighbours ($l = 6.28$ Å) in the xy plane (figure 15) by overlap of the $s\bar{p}_x p_z$ and the p_z' (or sp_z') orbitals of the interstitial atoms (I, I'). In the first case (p_z') the s^2 electrons of the I, I' atoms do not contribute, and the rest of the perpendicular p^2 electrons (p_y) yield an augmentation of the π bonds; this holds similarly for formation of sp_z' orbitals. In figure 16 the projection into the trigonal plane illustrates the inter-chain position of the interstitials. There are six equivalent sites around the three chain atoms per length c. This model appears to describe the most convenient and most effective interstitial position. It contributes an increase of binding between the trigonal chains and yields an additional parallel component in the trigonal direction. Hence, even for the existing dilution of the LID lines (core diameter small compared to the average distance), the stiffness of the crystal is increased by the defect contribution.

In the undisturbed crystal regions the $s\bar{p}_x p_z$ and $s\bar{p}_x \bar{p}_z$ hybrids are not occupied in our model, contributing an energy lowering in the LID by their occupation and overlap with the orbitals of the I, I' atoms (σ bonds). This demands a necessary electron redistribution within the trigonal chain electrons, leading to a withdrawal of electrons from the regular bonds, i.e. from the valence band. The amount of electron transfer depends on the energy balance of the total system. For transfer of a single electron per central chain atom, equation (14) is obtained, which allows a reasonable interpretation of the experimental results (e.g. figure 10). We guess that the counting of etch pits is too uncertain to allow a decision on a quantitative factor for the electron transfer. The model directly explains the electronic activity of the LID states and p-type conduction even at low temperatures.

6. Linear defect-induced energy sub-bands

The LID acceptor effect seriously influences the electronic properties of the as-grown

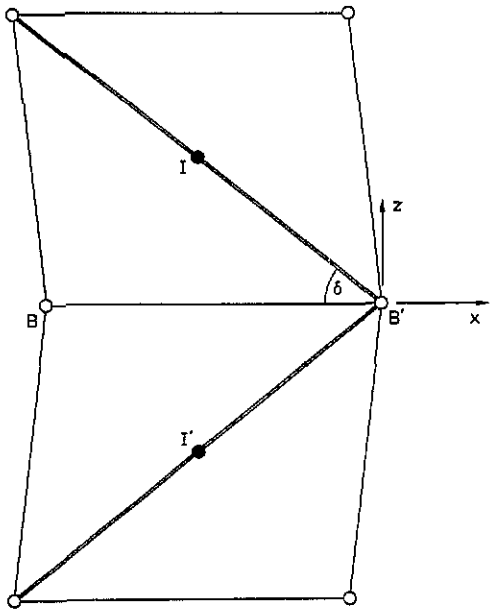

Figure 15. Tellurium atoms (○) (B, B', . . .) in the *xz* plane (perpendicular to the *xy* plane in figure 14) and proposed interstitial atoms (●) (I, I') within a linear defect structure ('*a* edge dislocation'). The double straight lines indicate additional, defect-induced σ bonds, two per interstitial atom. In the undisturbed lattice the distance $d_{B'I} = d_{B'I'} = 3.14$ Å and $\delta = 38.9°$ is deduced.

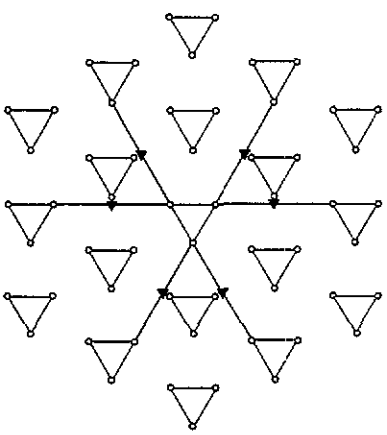

Figure 16. Projection of tellurium lattice into the trigonal plane in the range of a linear defect parallel to the trigonal axis. Regular lattice atoms (○) within the trigonal chains are connected by straight lines indicating the σ bonds. Around the core of the defect six interstitial atoms (▼) per length c contribute additional σ bonds between second nearest trigonal chains (———). For discussion, see text.

semiconductor tellurium. In the direction of the linear defect, the distance of the interstitial atoms is less than the de Broglie wavelength of the electrons transferred from the valence band into the LID states, leading to an overlap of the wavefunctions and formation of an 'impurity' energy band with a quasi-one-dimensional energy dispersion for electronic motion in the z direction. The number of interstitial atoms per unit length determines the degeneracy of the k_z states. The symmetry of tellurium renders a consideration of spin superfluous (Grosse 1969).

Occupation of the quasi-one-dimensional (QID) 'impurity' band allows one to explain the quasi-metallic behaviour of Te at temperatures below 1 K (see e.g. von Klitzing 1977). The dominant influence of the temperature-independent surface conductivity does not permit a comprehensive interpretation (Englert *et al* 1977). This would demand much higher surface hole concentrations than deduced by Silbermann (1975) from surface hole magneto-quantum oscillations.

The binding states between the interstitial and the regular Te atoms, in energy balance with the valence band states, are assumed here as partially filled, due to partial overlap of their energy spectra depending on the occupation of the LID states. This will be shown below. The non-occupied LID states are described as holes within a cylindrical 'impurity' potential, where the cylindrical coordinates $\rho, \varphi, z\ (e_z \| c)$ are most convenient. Hence, the potential energy V should depend on ρ only, and an effective-mass approximation may certainly be assumed. The Schrödinger equation becomes

$$\left[\frac{1}{\rho}\frac{\partial}{\partial\rho}\left(\rho\frac{\partial}{\partial\rho}\right)+\frac{1}{\rho^2}\frac{\partial^2}{\partial\varphi^2}-\frac{\partial^2}{\partial z^2}-\frac{2m^*}{\hbar^2}V(\rho)\right]\psi=-\frac{2m^*}{\hbar^2}E\psi. \tag{15}$$

The product *ansatz* $\psi(\rho, \varphi, z) = R(\rho)\phi(\varphi)Z(z)$ permits separation, i.e.

$$\frac{1}{\phi}\frac{\partial^2}{\partial\varphi^2}\phi=\text{constant} \qquad \frac{1}{Z}\frac{\partial^2}{\partial z^2}Z=\text{constant} \tag{16}$$

have to hold, respectively, yielding solutions of the form

$$\phi=(2\pi)^{-1/2}\,e^{il\varphi} \qquad Z=(2\pi)^{-1/2}\,e^{ik_z z} \tag{17}$$

where $l = 0, \pm1, \pm2, \ldots$. For $L_z = (\hbar/\mathrm{i})\partial/\partial\varphi$ (the component of angular momentum in the z direction) $l\hbar$ is obtained, and parallel to z a quasi-free translatory motion is possible (k_z). Hence, for the radial dependence, equation (15) may be written as

$$\frac{1}{R}\rho\frac{\partial}{\partial\rho}\left(\rho\frac{\partial}{\partial\rho}\right)R-l^2-k_z^2\rho^2+\frac{2m^*}{\hbar^2}[E-V(\rho)]\rho^2=0. \tag{18}$$

The potential energy $V(\rho)$ depends on the number N^* of charged I (I') atoms per length, their distance d and the lattice constant c along the trigonal axis (Read 1954) as

$$V(\rho)=-(e^2N^*d/c)f(\rho) \tag{19}$$

where $f(\rho)$ is influenced by screening and should be logarithmic (Labusch and Schröter 1980). In this case equation (18) cannot be solved analytically. For a qualitative discussion the assumption of a cylindrical potential well is convenient:

$$\begin{aligned} V(\rho)&=-V_0 \qquad &&\text{for } \rho\leqslant\lambda \\ V(\rho)&=0 \qquad &&\text{for } \rho>\lambda \end{aligned} \tag{20}$$

where $V_0 \sim N^*$ holds. Abbreviating $E - \hbar^2k_z^2/(2m^*)$ by E^*, equation (18) becomes, for $\rho \leqslant \lambda$,

$$\frac{\partial^2R}{\partial\rho^2}+\frac{1}{\rho}\frac{\partial R}{\partial\rho}+\left(\frac{2m^*}{\hbar^2}(V_0+E^*)-\frac{l^2}{\rho^2}\right)R=0. \tag{21}$$

This differential equation of Bessel type possesses a solution

$$R(\rho)=AI_l(K\rho)$$

where A is a normalization constant, I_l the Bessel function of order l and $K^2 = 2m^*(V_0 + E^*)/\hbar^2$ (I_l is finite for $\rho = 0$).

The wavefunction of equation (21) for finite $V(0)$ becomes

$$\psi = A^* I_l(K\rho)\, e^{il\varphi}\, e^{ik_z z} \tag{22}$$

where A^* is determined by normalization. The boundary conditions demand that ψ and its derivatives are also continuous for $\rho = \lambda$. In the approximation of equation (20) this is achieved for a vanishing wavefunction at $\rho = \lambda$, $\psi(\lambda) = 0$, which is certainly a reasonable approximation only for large binding energies. The zeros of the Bessel function $I_l(K\rho)$ at $\rho = \lambda$ hence yield the solutions. For $l = 0$ the argument $K\lambda$ is 2.4, 5.5, . . . , and for $l = \pm 1$ one obtains $K\lambda = 3.85, 7.0, \ldots$. The energy E^* becomes

$$E^* = \hbar^2 K^2/2m^* - V_0 \tag{23}$$

and describes the energy levels of the charge carriers in the QID potential well, e.g. of holes in the negatively charged LID. The ground state corresponds to $l = 0$; the first excited state is two-fold degenerate ($l = \pm 1$).

Von Ortenberg (1973a) calculated the energy levels of a quasi-free charge carrier in a linear short-range potential with parallel magnetic field. He showed that only the level with $l = 0$ is essentially influenced by the potential; for $l \neq 0$ no significant deviations from the regular Landau levels outside the 'impurity' potential were found. Equivalently, for $B \rightarrow 0$, exclusively the state with $l = 0$ and $K\lambda = 2.4$ (equation (23)) should be bound significantly, while the levels with $|l| = 1$ and $K\lambda = 3.85$ should have an exclusively weak interaction. This corresponds to a position of the $l = 0$ state in the tellurium energy gap and approximate coincidence of the $|l| = 1$ states with the valence band edge. The ionization energy in this approximation is deduced as

$$W_{\text{ion}} = \Delta E_{10}^{*0} = E^*(|l| = 1; K\lambda = 3.85) - E^*(l = 0; K\lambda = 2.4) = 3.1 \text{ meV} \tag{24}$$

for $m^* = m_\perp = 0.11\, m_0$ (Grosse 1969) and $\lambda = 2a_0^* = 32$ nm. Therefore, the lowest $l = 0$ LID level might correspond to the 'dislocation-induced' level postulated by von Alpen *et al* (1973) 3 meV above the valence band edge (the density of states of the LID sub-bands should be inversely proportional to the square root of the energy with respect to the level energy of concern, as a result of the k_z dispersion). The results deduced here are also supported by the experiments and simulations of Takita *et al* (1971, 1973), where an impurity conduction band near the valence band edge of Te was postulated. As a result of large screening of the LID, the k_z dispersion of the defect states may be assumed to be very similar to that of the tellurium valence band.

Within a magnetic field parallel to the LID ($\boldsymbol{B} \| \boldsymbol{e}_z$), in the effective-mass approximation the Hamiltonian operator

$$\mathcal{H} = [1/(2m^*)](\boldsymbol{p} - e\boldsymbol{A})^2 - V(\rho) \tag{25}$$

with symmetric gauge $\boldsymbol{A} = \frac{1}{2}B\rho\boldsymbol{e}_\varphi$ yields for the Schrödinger equation

$$\left(-\frac{\hbar^2}{2m^*}\Delta + V(\rho) - \frac{e}{2m^*} BL_z + \frac{e^2B^2}{8m^*}\rho^2 \right) \psi = E\psi \tag{26}$$

with $\mathcal{H}_0 = -(\hbar^2/2m^*)\Delta + V(\rho)$ for $B = 0$. Abbreviating the sub-band energies by E^0_{l,k_z} for $B = 0$, the low-field problem becomes (neglecting B^2 terms)

$$\begin{aligned} &[\mathcal{H}_0 - (e/2m^*)BL_z]\psi = E\psi \\ \text{and} \quad &E_{l,k_z} = E^0_{l,k_z} - \tfrac{1}{2}\hbar\omega_c l \end{aligned} \tag{27}$$

with $\omega_c = eB/m^*$. For $l = 0$ there is no influence of B; for $l = \pm 1$ paramagnetic ($l = +1$)

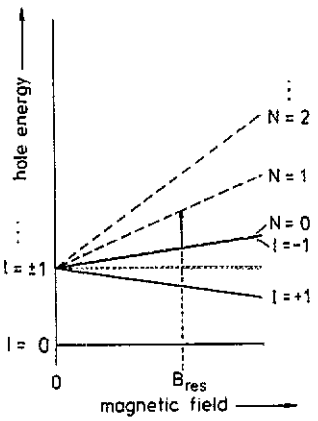

Figure 17. Energy levels for $k_z = 0$ of crystal holes (N) and defect states (l) as a function of magnetic field. The arrow at $B = B_{res}$ indicates a possible cyclotron resonance inactive-mode transition. For discussion, see text.

and diamagnetic ($l = -1$) contributions are contained. For high magnetic fields $V(\rho)$ may be neglected and the regular Landau sub-bands are obtained,

$$E = (N + \tfrac{1}{2})\hbar\omega_c + \hbar^2 k_z^2/2m^* \qquad \text{with } N = 0, 1, 2, \ldots . \tag{28}$$

The states with Landau quantum number N are degenerate in the angular momentum quantum number l, i.e. at high magnetic fields the levels for $l = +1$ and $l = -1$ coincide, in contrast to the case at low magnetic fields (equation (27)). However, for the situation of Te and magnetic fields of some teslas, the diamagnetic B^2 term in equation (26) has to be considered in the intermediate range.

One of the most striking linear defect-induced (i.e. by '*a* edge dislocations') properties of tellurium is the cyclotron resonance inactive inactive-mode (CRI) absorption (von Ortenberg and Button 1972, von Ortenberg *et al* 1972, von Ortenberg 1973b, Gerstenhauer *et al* 1979). The intensity of absorption depends on the density of the '*a* edge dislocations' (Gerstenhauer *et al* 1979). It occurs even at the lowest concentrations, where alignment of the etch pits in linear defect 'walls' does not exist (in our experiments this could be avoided up to about $N_{dis} = 10^7\ cm^{-2}$, which was also confirmed by Broniatowski and Faivre (1974) and Farvaque *et al* (1972)). Therefore, an explanation in terms of somewhat differing ε_{xx} and ε_{yy} components (perpendicular to the c axis) of the dielectric tensor, induced by defect walls, does not appear to be universal, in particular, for samples with CRI absorption and statistical distribution of the linear defects, which was actually observed.

Therefore, an interpretation by the LID states (as discussed above) is necessary. A transition (absorption) from the LID state $l = -1$ (sub-band, respectively) into the levels of the Landau sub-band with $N = 1$ of the undisturbed crystal (also containing states with quantum number of angular momentum $l = 0$) would allow fulfilment of the selection rule $\Delta l = +1$, which for $\boldsymbol{E} \perp \boldsymbol{B}$ and Faraday configuration corresponds to the σ^+ (or CRI) absorption. A level scheme for the CRI absorption is shown in figure 17. As a result of the differing radial wavefunctions for the initial (LID) and final states (Landau levels in Te), this transition should actually be allowed.

An argument against this interpretation would be the fact that CRI absorption for laser energies between 3.67 and 10.5 meV occurs at different magnetic fields, but at almost the same values as the cyclotron resonance active-mode (CRA) absorption in each case, which should not apply, when in the range between high and low magnetic fields

the B^2 term in equation (26) contributes to a greater or lesser extent. For lowest (equation (27)) and highest fields (equation (28)) the postulate would be fulfilled.

The solution of the problem is obtained when one considers the fact that the external magnetic field (vector potential) cannot influence the electrostatic balance (scalar potential) of charging and discharging of the LID and valence states, leading to an increase of binding of the crystal species of concern (including the LID). Therefore, a shift of the respective states relative to each other, induced by the magnetic field (B^2 term in equation (26)), should be accompanied by a charge transfer between the LID and valence band states which, in turn, leads to a modification of V_0 (equation (20)) and $V(\rho)$ (equation (19)) entering into K and E^* (equation (23)). Since the $E(k_z)$ dispersion in the valence band and the LID sub-bands may be assumed to be approximately the same, a relative fixing of both systems by a minimum of charge transfer leads to a variation linear in B only between the $l = -1$ states within the LID and $N = 1$ Landau levels of the valence band for the same k_z, yielding a magnetic field dependence as for a regular CRA absorption. Consequently, an unconstrained and universal explanation for the CRI absorption in Te, induced by the LID ('*a* edge dislocation'), is achieved for the first time. It is a consequence of the possibility of quasi-continuous charging of the LID, accompanied by an equivalent energy shift, which is not feasible for a quasi-zero-dimensional 'point' defect.

7. Magneto-impurity effects under non-ohmic conditions

Impurities in tellurium are of particular interest, since the preparation of 'pure' crystals is difficult in order to allow systematic doping. Under hot carrier conditions sharp structures are revealed in the magnetoresistance, showing additional fine structure for a finite component of $\boldsymbol{B}$ parallel to $\boldsymbol{c}$ (von Klitzing 1972, 1977, 1978). Von Klitzing interprets the extrema in the magnetoresistance by a resonance between the lowest acceptor excitation energy and another sharp energy, and suggests for the energy loss a phonon with energy 1.3 meV of unknown origin. Eaves and Portal (1978) propose an inter-valley LA phonon between the extrema at k_m (along the trigonal axis k_c) of the valence band $E(k)$ relation of camel's back shape in K_c direction. All the authors mentioned discuss the effect of different impurity levels, but cannot account quantitatively for the angular dependence of the resonance structure. The equidistance of the four-fold 'fine structure' is explained by Eaves and Portal 1979) on the arbitrary assumption that the g-factors for the Zeeman splitting in the bonding and antibonding states of the shallow acceptors should be one-half of the excited states. It is necessary, therefore, to check the compatibility of the results with our LID model.

The crystals investigated by von Klitzing (1972, 1977, 1978) were doped systematically with group V elements (Bi, Sb, As), possessing hole concentrations of some 10^{14} cm^{-3} at liquid-helium temperatures. For this doping level, the structures in the magnetoresistance are most distinct. The current direction was chosen arbitrarily as $\boldsymbol{J} \perp \boldsymbol{c}$; the magnetic field orientation was varied between transverse and longitudinal configurations. The magnitude of the electric field was adjusted (for a maximum effect) to some volts per centimetre. The resonance structures in the magnetoresistance occur between about 1 and 4 T magnetic induction, depending on the orientation of $\boldsymbol{B}$ relative to $\boldsymbol{c}$. The experiments were performed in a liquid-helium bath below $T_\lambda = 2.17$ K. Our proposal is the occurrence of scattering of the charge carriers into LID states and coupling

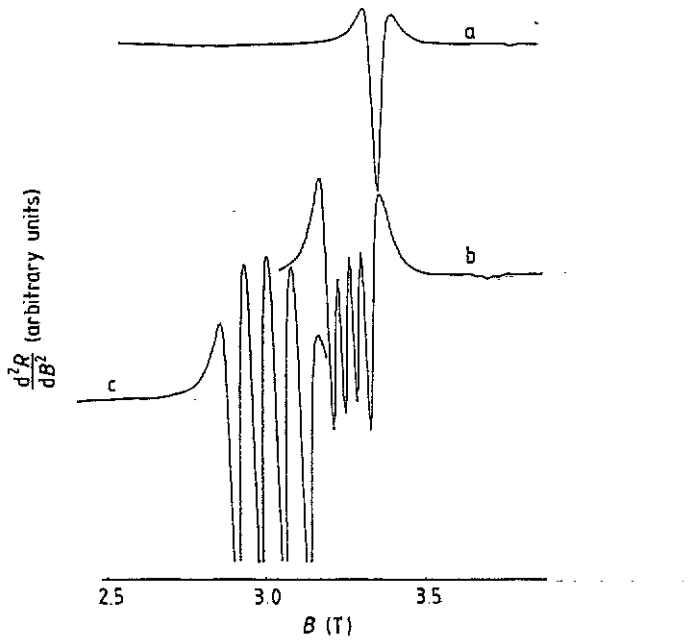

Figure 18. Second derivative of the sample resistance R with respect to B under hot hole conditions for $j \perp c$ of a Bi-doped crystal (HwTe 75) at 1.6 K and $90° - \vartheta = 0°$ (a), 5° (b) and 10° (c) (reproduced from figure 10 of von Klitzing (1977)).

to the inter-valley LA phonons perpendicular to the current direction. Thus the equidistant fine structure results from the occupation of the interstitial sites preferably by group V atoms (under the particular doping conditions), which are energetically favourable during the crystal growth of optimized terms. An example of the resonance structures in d^2R/dB^2, to be discussed below, is shown in figure 18 (figure 10 of von Klitzing (1977)).

The most pronounced four-fold, equidistant structure (figure 18) for $\boldsymbol{B} \| c$ is observed at $B \simeq 1.25$ T for the centre position (Bi, Sb doping; figure 4 of von Klitzing (1978)). Using cylindrical coordinates (ρ, φ, z; $e_z \| e_c$; section 5) the energy shift of the LID states in a tilted magnetic field ($\vartheta = \sphericalangle(\boldsymbol{B}, \boldsymbol{c})$) consists of ($\rho_{av} = 0$)

$$\Delta E = \tfrac{1}{2} l \hbar \omega_c \cos^2 \vartheta + \tfrac{1}{2} e^2 \rho_{av}^2 B_\parallel^2 / m_\perp + \tfrac{1}{2} e^2 \rho_{av}^2 B_\perp^2 / m_\parallel \tag{29}$$

where $\hbar\omega_c = \hbar eB/m_\perp$, $m_\parallel = (0.220 \pm 0.005) m_0$ and $m_\perp = (0.108 \pm 0.001)\, m_0$ (Couder *et al* 1973). According to the discussion above (section 6, equation (26)), the second term in equation (29) ($B_\parallel = B \cos \vartheta$) is compensated by a slight charge transfer between the valence band and the LID states, leading to figure 17 for $\boldsymbol{B} \| c$. Hence, the effective energy shift ΔE^* becomes ($B_\perp = B \sin \vartheta$)

$$\Delta E^* = \frac{\hbar e}{2m_\perp} l B \cos^2 \vartheta + \frac{e^2}{2m_\parallel} \rho_{av}^2 B^2 \sin^2 \vartheta \tag{30}$$

which contains the angular dependence deduced experimentally by von Klitzing (1978)

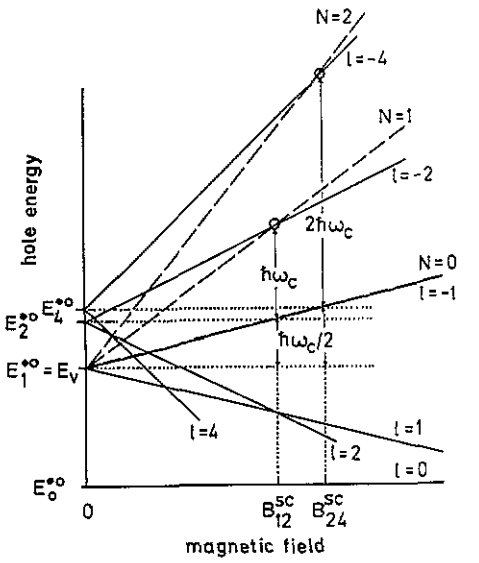

Figure 19. Equivalent energy level scheme for $k_z = 0$ as in figure 17 including the LID states with $l = \pm 2$ (E_2^{*0} for $B = 0$) and $l = \pm 4$ (E_4^{*0} for $B = 0$). At $B = B_{12}^{sc}$ the $N = 1$ and $l = -2$ levels coincide; at $B = B_{24}^{sc}$ the $N = 2$ and $l = -4$ states coincide. It is assumed that the valence band edge E_v (for $B = 0$) and E_1^{*0} (for $l = \pm 1$ and $B = 0$) have the same energy. For discussion, see text.

for the centre position of the magnetoresistance structure. The ratio $Q = \Delta E^*(\vartheta = 0)/\Delta E^*(\vartheta = 90°)$ yields

$$Q = \frac{\hbar m_\parallel}{m_\perp \rho_{av}^2 eB} l = \frac{m_\parallel}{m_\perp} l \frac{\hbar}{\rho_{av}^2 eB}. \tag{31}$$

For $\boldsymbol{B} \| \boldsymbol{c}$ and a macroscopic extension of the LID, $\rho_{av}^2 eB$ may be assumed semiclassically to amount to $\hbar$ for a bound oscillator ground state ($N = 0$), and hence Q becomes

$$Q = (m_\parallel / m_\perp) l. \tag{32}$$

Under hot carrier conditions and $\boldsymbol{j} \perp \boldsymbol{B}$, an excitation from the $N = 0$ to the $N = 1$ Landau sub-band has to be assumed. Such holes may be elastically scattered by the LID scatterers (for $N_{dis} \simeq 10^6$ cm^{-2} and $F \simeq 2$ V cm^{-1}, the average energy difference is $eF(N_{dis})^{-1/2} \simeq 2$ meV) into the $l = -2$ LID states under k_z conservation, if coincidence of the $N = 1$ and $l = -2$ levels (and sub-bands) occurs. The variation of angular momentum is $-\hbar$ when the $N = 1$ state belongs to angular momentum quantum number $l = -1$. The $N = 1$ and $l = -2$ coincidence applies for $\Delta E_{21}^{*0} = \frac{1}{2}\hbar\omega_c$ (figure 19). At the same magnetic field, $E^*(l = -2) - E^*(l = -1) = E^*(l = -1) - E^*(l = +1) = \hbar\omega_c$ (k_z constant) and allows an exchange of energy and angular momentum by relaxation of the excited LID hole ($l = -2$) to $l = -1$ and excitation of an $l = +1$ LID hole into the $N = 0$ ($l = 0$) Landau sub-band. The $N = 0$ hole may be excited again under hot carrier conditions; and the remaining $l = -1$ LID hole, excited from $l = +1$, is scattered by the inter-valley LA phonon by emission of $\hbar\omega_c$ for $l = -2$. The phonon energy need not be exactly $v_s 2k_m \hbar$ ($k_z = \pm k_m$ = extrema positions of valence band; v_s = sound velocity), since the hole $E(k_z)$ relaxation differs from that of the phonons.

For $\boldsymbol{B} \| \boldsymbol{c}$ and $B = 1.25$ T (approximate centre of four-fold structure), $\Delta E_{21}^*(B = 0) = \frac{1}{2}\hbar\omega_c = 0.67$ meV is smaller than (but comparable in order of magnitude to) the estimation for ΔE_{10}^{*0} (equation (24)). The ratio Q (equation (32)) has to be compared with the cyclotron energy for $\boldsymbol{B} \| \boldsymbol{c}$ and $\boldsymbol{B} \perp \boldsymbol{c}$, when coincidence of the $N = 1$

Landau and the $l = -2$ LID levels occurs for the resonant ($\Delta E_{21}^{*0} = \frac{1}{2}\hbar\omega_c$) scattering process. This ratio yields another factor $(m_\perp/m_\parallel)^{1/2}$, and hence the overall anisotropy

$$(m_\perp/m_\parallel)^{1/2} Q = (m_\parallel/m_\perp)^{1/2} l \tag{33}$$

for $|l| = 2$ becomes 2.85 ± 0.05, coincident with the experimental anisotropy value (2.82) deduced for antimony (von Klitzing 1978) with almost the same nuclear charge as tellurium. For As and Bi the effective masses in the LID states should deviate by a somewhat higher amount than for Sb, so that the corresponding anisotropies are somewhat smaller (Bi) or higher (As), respectively.

The four-fold, equidistant splitting of the magnetoresistance structure (ΔB) for $0 \leqslant \vartheta < 90°$ in our model results from the coupling between the LID states and the $J = \frac{1}{2}$ electronic configuration of the group V doping atoms within the LID, yielding combinations $|l \pm J|$, i.e. $\frac{5}{2}$ and $\frac{3}{2}$ for $l = \pm 2$ and $\frac{3}{2}$ and $\frac{1}{2}$ for $l = \pm 1$ (equivalently $\frac{1}{2}$ for $l = 0$). For the transition $l = -2$ to $l = -1$ the average transition energy $\hbar\omega_c$ is modified proportional to ± 3 and ± 1 times $B\cos^2\vartheta$ (equation (29)), yielding an equidistant splitting around the centre position of the magnetoresistance structure.

The second four-fold, equidistant structure in the magnetoresistance centred at $B = 1.6$ T for $\boldsymbol{B} \| c$ (von Klitzing 1978) may be discussed as a resonant scattering for coincidence of the $N = 2$ and $l = -4$ levels, where $\Delta E_{41}^{*0} = E_4^{*0} - E_1^{*0} = \frac{1}{2}\hbar\omega_c$ (for $B = B_{24}^{sc}$ in figure 19). Here, from $|l \pm J|$ for $l = -4$ and $l = -1$ ($J = \frac{1}{2}$) the splitting factors ± 6 and ± 2 yield the equidistant fine structure, and the relaxation by on average $2\hbar\omega_c$ causes a complementary excitation of two $l = +1$ holes into the $l = -1$ state. Therefore, the principal balance of energy and angular momentum is unchanged.

The relation for the splitting $\Delta B \sim B^4 \cos^2\vartheta$ (B = centre value of resonance fields) given by von Klitzing (1978) does not contain the explicit angular dependence of ΔB, since B is a function of ϑ, too. Substituting B^2 by equations (30) and (33), the relative splitting becomes, for $|l| = 2$,

$$\frac{\Delta B}{B} \sim \frac{B\cos^2\vartheta}{(4m_\parallel/m_\perp)\cos^2\vartheta + \sin^2\vartheta} \tag{34}$$

showing that the first term of equation (30) is compared with the total shift ΔE^* modified by the variation of the cyclotron energy with ϑ.

The possibility of a complete and quantitative explanation of the angular shift of the central position of the magnetoresistance structure by equation (30), of the anisotropy by equation (33) for scattering into $l = -2$ or -4 states (including the entire process of relaxation) and of the equidistant four-fold splitting and its angular dependence give further evidence for the universal applicability of the LID model assumed. The proposal demands an insertion of the group V doping atoms preferably into the LID sites, necessitating a balance between crystal seed quality (N_{dis}) and chemical doping level. High doping results in additional point impurities, covering the peculiarities of the QID superlattice structures in tellurium. This sheds light on the partially controversial discussions that have characterized the research on Te for a long time. The detailed interpretation of further hot carrier effects in tellurium is left to future work.

8. Conclusions

The thermoelastic effect is shown to be a sensitive tool for the investigation of the influence of defects on binding in inhomogeneously bound materials. The concentration

of linear defects parallel to the *c* axis ('*a* edge dislocations') yields a strengthening of binding. Simultaneously, the electronic activity of the linear defects leads directly to a model of interstitial atoms between the trigonal chains, contributing an improved binding between the chains and parallel to them. It allows one to explain, in addition, the quasi-metallic behaviour of the semiconductor tellurium at low temperatures. Also, the quasi-one-dimensional eigenstates of charge carriers in the cylindrical defect potential yield a direct possibility for the interpretation of CRI absorption induced by the linear defects, without postulation of a second optical axis for real tellurium (including '*a* edge dislocations') as suggested previously. Incorporation of group V doping atoms as interstitials in the linear defects allows one to explain the magneto-impurity effects observed in the hot carrier regime. This reveals that the preparation of perfectly doped crystals demands microscopic QID superlattice incorporation of the group V atoms during crystal growth with matching of the concentrations of LID sites and doping atoms.

Acknowledgment

The financial support of the Deutsche Forschungsgemeinschaft is appreciated.

References

Abokarov D A, Banyulis E Y, Bagduev G B, Ivanov G A, Polikhronidi N G and Chernobai V I 1973 *Fiz. Tekh. Poluprov.* 7 579
Blondke M 1975 *Diploma thesis* Würzburg
Broniatowski A and Faivre G 1974 *Phil. Mag.* **30** 765
Couder Y, Hulin M and Thomé H 1973 *Phys. Rev.* B 7 4373
Dato P and Köhler H 1984 *J. Phys. C: Solid State Phys.* **17** 3711
Doukhan J C 1971 *Doctoral thesis* Lille
Doukhan J C, Doukhan N, Saada G and Thomas B 1969 *Phys. Status Solidi* a **35** 835
Doukhan J C and Farvaque J L 1971 *Phys. Status Solidi* a **4** K1
Drope R 1968 *Diploma thesis* Köln
Eaves L and Portal J C 1979 *J. Phys. C: Solid State Phys.* **12** 2809
Englert T, von Klitzing K, Silbermann R and Landwehr G 1977 *Phys. Status Solidi* b **81** 119
Faivre G 1974 *Phil. Mag.* **29** 1289
Farvaque J L, Crampon J, Doukhan J C and Escaig B 1972 *Phys. Status Solidi* b **14** 623
Freitag G 1977 *Diploma thesis* Würzburg
Gerstenhauer E, Bauer G, Grosse P and Doukhan J C 1979 *Phys. Status Solidi* b **93** 629
Grosse P 1969 *Die Festkörpereigenschaften von Tellur* (*Springer Tracts in Modern Physics 48*) (Berlin: Springer)
Grosse P and Gerlach E 1979 *The Physics of Selenium and Tellurium* (*Solid State Sciences 13*) (Berlin: Springer)
Jamieson J C and McWham D B 1965 *J. Chem. Phys.* **43** 1149
Kalinski Z B and Lehmann G 1976 *Krist. Technik* **11** 281
Köhler H 1978 *Proc. 14th Int. Conf. Physics of Semiconductors 1978* (*Inst. Phys. Conf. Ser. 43*) (Bristol: Institute of Physics) p 553
Labusch R and Schröter W 1980 *Dislocations in Solids 5* (ed F R N Nabarro) (Amsterdam: North-Holland) p 127
Landeck K H 1977 *Diploma thesis* Würzburg
Naukkarinen K 1972 *Phys. Status Solidi* a **13** 399
Parthasarathy G and Holzapfel W B 1988 *Phys. Rev.* B **37** 8499
Read W T 1954 *Phil. Mag.* **45** 779 and 1119
Roos M 1975 *Diploma thesis* Würzburg
Silbermann R 1975 *Doctoral thesis* Würzburg
Swalin R 1972 *Thermodynamics of Solids* (New York: Wiley)

Takita K, Hagiwara T and Tanaka S 1971 *J. Phys. Soc. Japan* **31** 1469
Takita K, Suzuki K and Tanaka S 1973 *J. Phys. Soc. Japan* **34** 667
von Alpen U 1973 *Doctoral thesis* Aachen
von Alpen U, Doukhan J C, Escaig B and Grosse P 1973 *Phys. Status Solidi* b **55** 667
von Klitzing K 1972 *Doctoral thesis* Würzburg
—— 1977 *Thesis of Habilitation* Würzburg
—— 1978 *Solid-State Electron.* **21** 223
von Ortenberg M 1973a *Phys. Status Solidi* b **60** 273
—— 1973b *Phys. Status Solidi* b **60** 531
von Ortenberg M and Button K 1972 *Solid State Commun.* **11** 1315
von Ortenberg M, Button K, Landwehr G and Fischer D 1972 *Phys. Rev.* B **6** 2100